8-15-2011

Enhancement of Thermoelectric Efficiency by Uniaxial Tensile Stress in n-type GaAs Nanowires

Abhijeet Paul
Network for Computational Nanotechnology, Purdue University

Kai Miao
Network for Computational Nanotechnology, Purdue University

Ganesh Hegde
Network for Computational Nanotechnology, Purdue University

Saumitra Hehrotra
Network for Computational Nanotechnology, Purdue University

Mathieu Luisier
Network for Computational Nanotechnology, Purdue University

See next page for additional authors

2011 11th IEEE International Conference on Nanotechnology
Portland Marriott
August 15-18, 2011, Portland, Oregon, USA

Enhancement of thermoelectric efficiency by uniaxial tensile stress in n-type GaAs nanowires

Abhijeet Paul*, Kai Miao, Ganesh Hegde, Saumitra Mehrotra, Mathieu Luisier and Gerhard Klimeck
School of Electrical and Computer Engineering and Network for Computational Nanotechnology,
Purdue University, West Lafayette, Indiana-47906, USA.
Email: (paul1, kmiao, ghegde, smehrotr, mluisier, gekco)@purdue.edu

***Abstract*—The thermoelectric power-factor (PF) and efficiency (ZT) of GaAs nanowires (NWs) can be improved by (i) choosing a proper wire growth and channel orientation, (ii) by applying uniaxial tensile stress, and (iii) suitable wire cross-section size. In this work we study the impact of these three factors on the PF and the ZT. Tensile stress, channel direction and cross-section size allows bandstructure engineering to tune the electronic conductance (G) and the Seebeck coefficient (S). [110] GaAs NWs grown on (111) surface provide maximum PF (∼3X) and ZT (∼1.3X) compared to [100]/(100) NWs, which can be attributed to the G enhancement induced by the L valley contribution under strain.**

***Index Terms*—GaAs, uniaxial-stress, thermoelectricity, Tight-binding.**

I. INTRODUCTION

Inherent low thermal conductivity and high electron mobility can make GaAs a promising thermoelectric material [1], [2]. However, GaAs suffers from DOS bottleneck which results in low electron density [3] and hence low electronic conductivity (G). It has been shown experimentally that nanowires (NWs) can improve the thermoelectric efficiency (ZT) many times over bulk material [4] due to two main reasons, (i) strong reduction in lattice thermal conductivity (κ_l) [2], [5], and (ii) electronic DOS engineering allowing to increase the thermoelectric power factor (PF) [4], [6]. Both PF and ZT of a material are defined as [6],

$$PF = S^2 \cdot G \quad (1)$$

$$ZT = \frac{PF}{\kappa_e + \kappa_l} \cdot T, \quad (2)$$

where S, G, κ_e, κ_l and T are the electron Seebeck coefficient, electronic conductivity, electronic thermal conductivity, lattice thermal conductivity and temperature, respectively.

GaAs has 3 important conduction band valley minima, namely the Γ valley, the L valley and the X valley (Fig. 1). In relaxed bulk GaAs these valleys are well separated in energy (see Fig. 1) and electronic conduction dominantly takes place in the Γ valley which has a very small transport mass ($m*_{tr} \sim 0.067m_0$, where m_0 is free electron mass) but also has low DOS resulting in the 'DOS bottleneck'[3]. However, recent experimental work shows that uniaxial tensile stress can reduce this DOS bottleneck in GaAs by increasing the L valley contribution in the electronic transport [7]. Another recent proposal suggests the use of nanostructures grown on (111) surfaces to enhance DOS by confining one of the L valleys [8]. Guided by these experimental and theoretical work, we

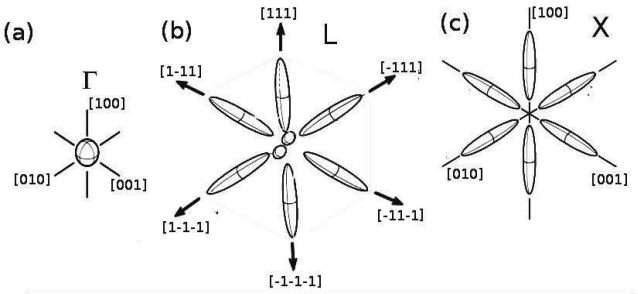

Valley	Γ	L	X
ΔEc (eV)	0	0.28	0.47
m^*_l/m_0	0.067	1.9	1.3
m^*_t/m_0	0.067	0.075	0.22

Fig. 1. Three important conduction valleys in bulk GaAs, (a) Γ valley, (b) L valley and, (c) X Valley. The important masses and the energy difference (ΔE) of the valleys from the Γ valley are also shown.

conducted a theoretical study to understand the impact of (a) channel and growth direction (X/Y), (b) uniaxial strain, and (c) cross-section size on the thermoelectric power factor and the ZT of n-type GaAs NWs.

The advancement in the process technology now allows the fabrication of high quality pure GaAs nanowires as well as core-shell nanowires. Some of the important fabrication processes are, (i) vapor-liquid-solid (VLS) technique for both n and p-type wires [9], [10], (ii) molecular beam epitaxy (MBE) [11], [12], and (iii) solid phace nanowire growth [13]. Thus, better quality GaAs nanowires can be used for manufacturing thermoelectric modules.

This paper has is organized as follows. Thermoelectric theory and the calculation procedure are described in Sec. II. The results on the thermoelectric (TE) properties in n-type GaAs nanowires (GaAs-NW) are discussed in Sec. III followed by the conclusions in Sec. IV.

II. THEORY AND APPROACH

The calculation of the electronic TE parameters (G, S and κ_e) is done using the Landauer's approach [14]. This method has been shown to capture the transport properties in mesoscopic systems very well both in the ballistic as well as in the diffusive regime [15], [6]. Landauer's approach also works well in moderate to high temperature regime [6] making it a very robust formulation. The electron scattering in these n-

type GaAs nanowires is taken into account by using a diffusive form of the Landauer's model [6].

The value of the electronic conductance (G), the Seebeck coefficient (S) and electronic thermal conductance (κ_e) at a given temperature T are obtained as [6],

$$G = \frac{2q^2}{h} \cdot I_0 \quad [\Omega^{-1}] \tag{3}$$

$$S = -[k_B/q] \cot[I_1/I_0] \quad [V/K] \tag{4}$$

$$\kappa_e = [\frac{(2Tk_B^2)}{h}] \cdot [I_2 - (I_1^2/I_0)] \quad [W/K] \tag{5}$$

$$I_j = \int_{E_{min}}^{E_{max}} \Big[\frac{(E-E_F)}{k_BT}\Big]^j \cdot \mathcal{T}(E) \cdot \mathcal{M}(E) \cdot \frac{-\partial \mathcal{F}_{FD}}{\partial E} \cdot dE, \tag{6}$$

where, q is the electronic charge, h is Planck's constant, k_B is Boltzmann's constant, E_F is the electron Fermi energy level and $\mathcal{F}_{FD}$ is the Fermi-Dirac distribution for the electrons at a temperature T. The terms $\mathcal{M}(E)$ and $\mathcal{T}(E)$ represent the electronic density of modes (DOM) and transmission of the mode at a given energy E, respectively [6]. An important point to note here is that DOM depends only on the electronic dispersion whereas the transmission depends both on the dispersion as well as the scattering mechanisms present in the system.

Under ballistic transport $\mathcal{T}(E)$ is taken to be 1 at all the energies, however, under diffusive case this can be calculated as [6],

$$\mathcal{T}(E) \approx \frac{\langle\langle \lambda(E) \rangle\rangle}{Lch}, \tag{7}$$

where $\langle\langle \lambda(E) \rangle\rangle$ represents the average electronic mean-free-path (MFP) and Lch is the length of the conductor between the two contacts. The value of the MFP is governed by the scattering mechanisms present in the system and can be obtained for a 1D conductor in the following way [6],

$$\langle\langle \lambda(E) \rangle\rangle = 2 \cdot \frac{\sum_{k_x} v_x^2(k_x, E) \cdot \tau_{scat}(k_x, E)}{\sum_{k_x} |v_x(k_x, E)|}, \tag{8}$$

where $v_x(k_x, E)$ is the electron group velocity at an energy E with momentum k_x. The term τ_{scat} is the scattering time constant dependent on both E and k_x. The summation is over all the periodic 1D k_x vectors. In the present calculation we assume the scattering time constant to be isotropic in k_x and constant in E , $\tau_0 = \tau_{scat}(k_x, E)$. This simplifies Eq. 8 to,

$$\langle\langle \lambda(E) \rangle\rangle = 2 \cdot \tau_0 \cdot \sum_{k_x} v_x(k_x, E). \tag{9}$$

The constant τ assumption works well when the scattering mechanisms are assumed to be dominated by the acoustic and the zone center optical phonons (which are proportional to the electronic DOS) [16], [17]. The value of τ_0 is chosen such that the electron mobility (μ_e) for a 6nm X 6nm square relaxed GaAs-NW comes out to be around 1200 $cm^2/V.s$ at an inversion charge density (N_s) of $10^{12} cm^{-2}$ (Fig. 2). The bulk GaAs μ_e reported in the literature, at this Ns, varies between 7100 to 2000 [11]. However, we choose a lower mobility value to account for the additional defects that can present in the nanowires like surface roughness (SR), impurities, etc [16]. The value of τ_0 = 1 femto second (fs) is used in all the calculations.

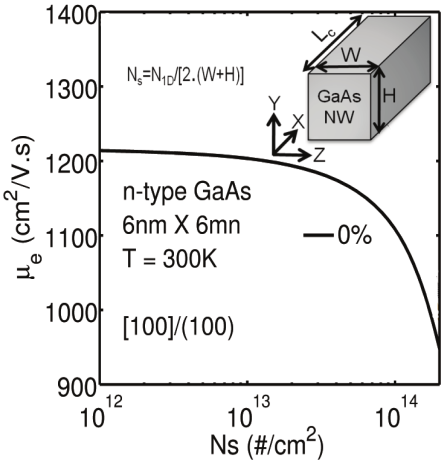

Fig. 2. Electron mobility calibration for GaAs nanowire of 6nm X 6nm cross-section size at T=300K.

The correct calculation of the DOM in ultra-scaled GaAs NWs relies on an accurate electronic bandstructure model. In the present study we use an atomistic 20 band $sp^3d^5s^*$ tight-binding (TB) model [18], [19] which accounts for (the exact atomic positions, orientation, shape, size and strain effects in the NWs. To properly model the band curvature (related to eff. mass) and the band off-sets for the X and L valleys in GaAs, a new set of TB parameters have been obtained which will be published elsewhere.

A. NW details

Atomistic square GaAs NWs with intrinsic channel are studied with specific channel (X) and growth (Y) directions for a given width (W) and height (H=W) (Fig. 3). Six different combinations of [X]/(Y) are considered for these NWs (Table I) with W ranging from 2 to 6 nm. Uniaxial tensile strain (ϵ_{xx})

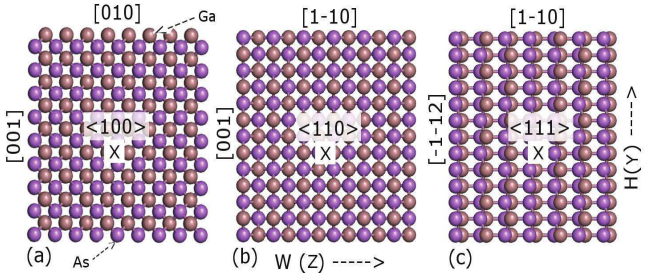

Fig. 3. Three projected unit cells (out of six considered in this work) of GaAs NWs with W = 3nm (Table I). Y is the growth direction whereas X is the transport direction. (a) dev. I [100]/(100), (b) dev. III, [110]/(110), and, (c) dev. IV [111]/(110). The side wall orientations are also shown.

TABLE I
DETAILS OF THE CHANNEL ORIENTATION (X) AND THE GROWTH DIRECTION (Y) FOR GAAS NWS USED IN THIS STUDY.

NW label	I	II	III	IV	V	VI
Channel [X]	[100]	[1-10]	[1-10]	[1-11]	[001]	[011]
Growth (Y)	(100)	(111)	(110)	(110)	(110)	(100)

values used are 0, 0.5, 1, 2, 3 and 5% along the X direction. All the device terminal characteristics are calculated at T = 300K.

III. RESULTS AND DISCUSSION

Uniaxial strain modifies the electronic density of states (DOS) which can affect both the electronic transport properties as well as the electronic scattering rates. The enhancement in the thermoelectric PF and ZT is optimized by the interplay of proximity of the Γ-L valley and scattering of the electrons in these valleys. The three engineering knobs which are controlled to optimze the thermoelectric performance in n-type GaAs nanowires are (i) uniaxial strain(STR), (ii) cross-section size (CS) and, (iii) wire orientation (OR).

The effect of the three factors (A,B and C) on the transport properties is captured by the DOM whereas the scattering effect for each mode is captured by the transmission ($\mathcal{T}$) (Eq. 6 and 7). The effective DOM (DOM×$\mathcal{T}$) for all the devices with 6nm × 6nm cross-section are shown for the relaxed and 5% uniaxial tensile strain case in Fig. 4 a and b, respectively. For the unstrained case all the devices show similar effective DOM (Fig. 4 a). For the strained case the effective DOM starts at a lower energy since the conduction bands (CB) shift downwards in energy under tensile strain(Fig. 4b). Devices II, III and VI show a 4× increase in the effective DOM which eventually improves the thermoelectric PF in these nanowires (Fig. 4b).

Uniaxial tensile stress improves the maximum thermoelectric PF in both 3nm and 6nm cross-section size wires as shown in Fig. 5. For 3nm wires the maximum improvement is obtained in device VI under 5% strain (3.6×) as compared to the unstrained device (Fig. 5a). Devices II and III also show ∼2.2× increase in the PF (Fig. 5a). These three devices also

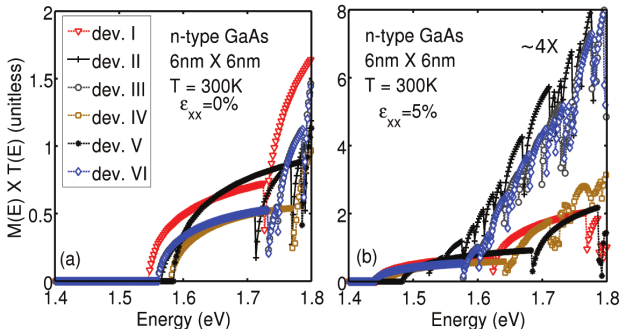

Fig. 4. Number of modes in all the 6 types of nanowires with cross-section size 6nm × 6nm under (a) relaxed condition, and (b) uniaxial strain. The number of modes in dev. II, III and VI increases by ∼4× under strain.

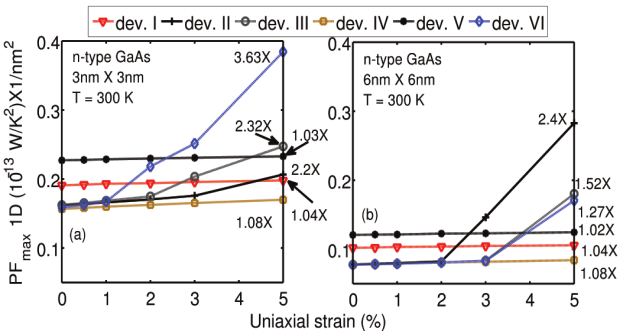

Fig. 5. Thermoelectric PF variation with uniaxial strain in (a) 3nm × 3nm and (b) 6nm × 6nm cross-section size GaAs-NWs for all the 6 device types (Table I).

show improvement of ∼2.5-1.5× for 6nm wires (Fig. 5b). The enhancement in the PF for these three devices is obtained by the increased contribution of the L valley to the conductance (G) under uniaxial tensile stress along with the Γ valley [7]. Smaller wires show larger improvement in PF due to reduced scattering effect on G as the valleys (Γ-L) are further apart in energy compared to the 6nm wires.

The impact of the wire cross-section size on the PF is shown in Fig. 6. As the wire cross-section size reduces the G per unit area increases since the number of conducting channels become constant for small diameter wires. This results in an increase in the PF per unit area for smaller wires. Under the unstrained case device I (where the Γ valley dominates the electronic transport) shows the maximum PF (Fig. 6a). However, application of the uniaxial stress can increase the influence of the L valley on G which improves the overall PF (Fig. 6b). Device II, III and VI show improvement in the PF even though the scattering also increases since the CB valleys move closer under strain. *Thus, with the proper choice of orientation and wire cross-section size the PF of the n-type GaAs-NWs can be improved even in the presence of electron scattering*.

The increase in the peak PF can be understood from the behavior of the individual components of the PF (S and G) under different strain, cross-section size and orientation. The

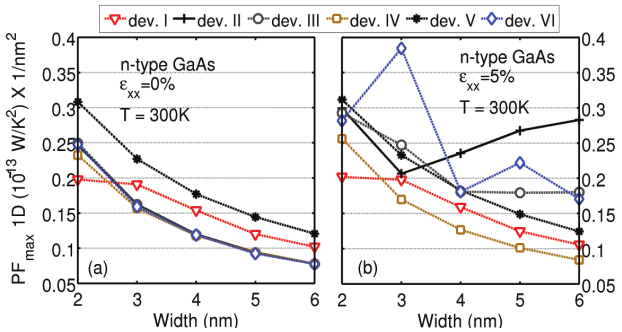

Fig. 6. Variation in the peak PF for n-type GaAs-NWs with cross-section size for all the devices types for (a) unstrained case and (b) strained case with 5% uniaxial strain.

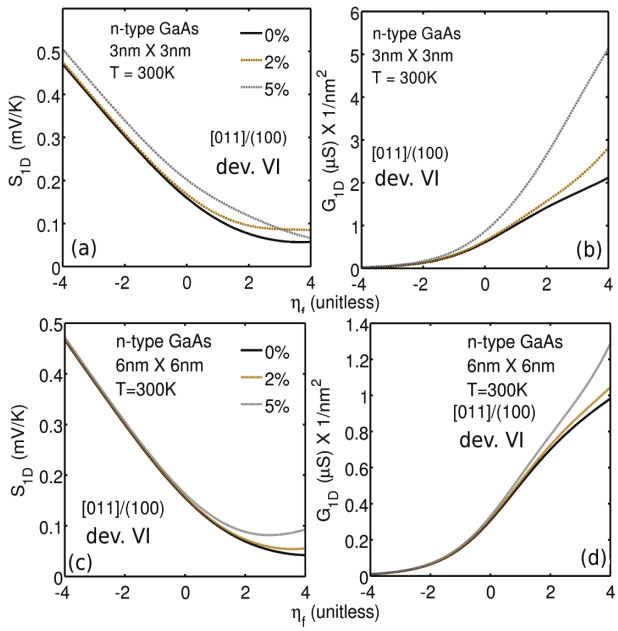

Fig. 7. Variation in S and G with strain for various reduced Fermi-level positions ($\eta_f = (E_C - E_F)/k_BT$). Variation in (a) S, and (b) G for 3nm $\times$ 3nm NWs for 3 different uniaxial strain values (0, 2 and 5%). Similar variation in (c) S, and (d) G for 6nm $\times$ 6nm NWs for three strain levels.

S and G value for device VI are shown in Fig. 7 since in these wires the PF improves for all the cross-section sizes (2nm to 6nm). For 3nm $\times$ 3nm both S and G improve with unixial tensile strain (Fig. 7a, b). However, S and G improvements originate from different physical processes. The CB valleys (both Γ and L) come closer to the Fermi level under tensile strain which increases the value of S. The value G improves since the CB valleys are optimally separated in energy to provide more conducting channels for electrons and also suppresses the inter-valley scattering (Fig. 7 a and b). However, the larger wires (6nm cross-section size) show insignificant improvement in S and G with strain (Fig. 7 c and d). *Thus, uniaxial tensile strain improves the peak PF more in smaller wires compared to the larger wires.*

The enhancement in the PF also helps in improving the ZT. The thermoelectric figure of merit (ZT) is calculated at T=300K using the electronic properties obtained from Landauers approach [14] and lattice thermal conductivity (κ_e) of 1W/m-K as reported for GaAs NWs [1], [5]. It is important to note that ZT depends on the total thermal conductivity which is contributed by the lattice (κ_l) and the electrons (κ_e). The peak PF and the peak ZT value are obtained at different values of the reduced Fermi-level (η_f) (Fig. 8). The PF is maximum when the product of S and G is the highest. The peak ZT value is obtained when the ratio of the PF and total thermal conductivity ($\kappa_l + \kappa_e$) is the highest.

The variation in the ZT with strain for device I and VI with a cross-section size of 6nm $\times$ 6nm is shown in Fig. 9. Under identical strain condition(ϵ_{xx} = 5%) device I and device VI show very small ZT enhancement (5-7%) (Fig. 9). The

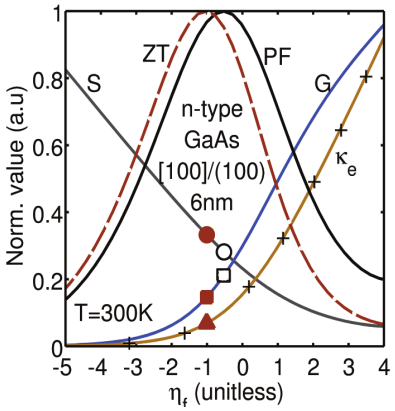

Fig. 8. Variation of the various transport parameters with η_f for device I with a 6nm $\times$ 6nm cross-section size. The peak ZT and the peak PF are obtained at slightly different Fermi-levels.

reason for these small enhancement in these two devices are different. In device I, the Γ valley dominates the electronic transport which results in smaller G (DOS bottleneck) and hence smaller ZT. Whereas, for device VI though the Γ and L valleys come close to each other under strain, the inter-valley scattering suppresses G which results in a small increase in the ZT. Thus, larger wires do not show significant improvement in the peak ZT value with uniaxial tensile strain.

Figure 10 shows the peak ZT variation with strain for different devivces. Smaller nanowires show higher ZT value (around 2-2.5) compared to the larger nanowires (around 1.5-1.1) due to larger PF. Device VI shows $\sim$36% enhancement in the peak ZT for smaller wires for 5% strain (Fig. 10a). This improvement in device VI becomes possible due to the suppression of the inter-valley scattering in the smaller wires governed by the optimal energy separation of the Γ-L valleys because of the geometrical confinement. For 6nm NWs, device II shows $\sim$14% improvement in the peak ZT value for 5% unixial tensile strain. *Thus, smaller wires show larger gain in ZT under strain due to the reduced inter-valley scattering of the electrons.*

The complete effect of strain and cross-section size on the

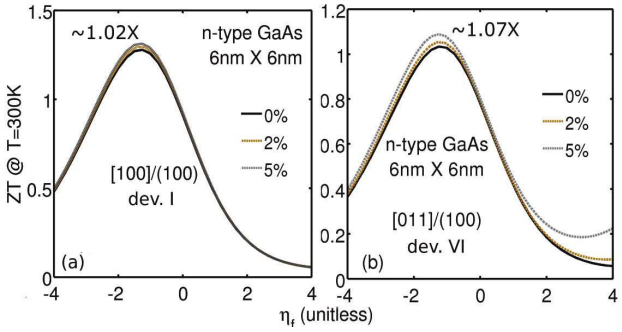

Fig. 9. ZT variation for 6nm $\times$ 6nm GaAs NW with strain for (a) device I, and (b) device VI. A resonably good ZT of $\sim$1 at T=300K is obtained for both the devices. The enhancement with strain is around 4% and 7% in device I and VI, respectively.

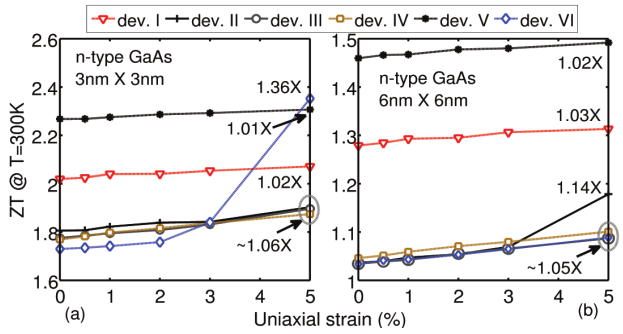

Fig. 10. Variation in the peak ZT at 300K for all the devices with uniaxial strain with cross-section size of (a) 3nm × 3nm, and (b) 6nm × 6nm. A reasonable good ZT of ∼ 1 is obtained for all the 6nm wires which increases upto 2 for 3nm wires. Device II and VI show good enhancement in the peak ZT with strain.

peak ZT is provided in Fig. 11 for device I and VI. The ZT value varies from ∼1 for 6nm size wires to ∼2.5 for 2nm size wires. Under uniaxial tensile strain the enhancement in ZT is higher for device VI compared to device I due to the increased contribution of the L valley to the conductance. Improvement in the ZT with uniaxial tensile strain is larger for smaller wires due to reduced electron scattering. The absolute ZT values may further reduce due to surface roughness scattering of electrons which has not been included in the present study. However, the order and the trend of the ZT is expected to remain the same. The complete effect of the orientation, cross-section size and the strain for optimal value of PF and ZT are summarized in Table II.

IV. CONCLUSION

The possibility of n-type GaAs NWs to serve as the next generation thermoelectric material has been shown. A proper choice of growth and channel orientation along with uniaxial stress and cross-section size provides a good way to enhance both the PF and the ZT of GaAs NWs. A 5% uniaxial tensile stress can improve the PF and ZT by ∼3× and ∼1.14×, respectively in 6nm NWs which further increases with W scaling. The GaAs-NWs grown on (110) or (111) surfaces

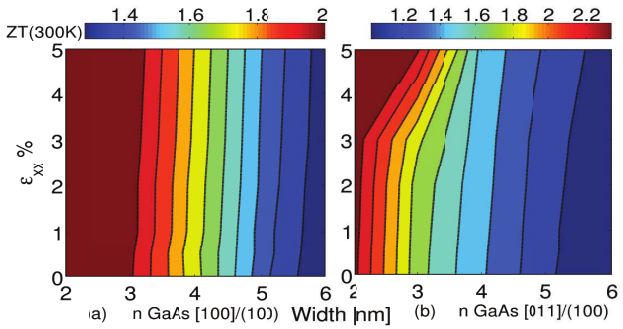

Fig. 11. A 2-D contour plot for the variation in the peak ZT for (a) device I, and (b) device VI for different cross-section sizes and strain levels. The smaller wires show better enhancement in the peak ZT as strain is applied which is due to the optimal proximity of the valleys to enhance S and G yet keeping the scattering rates low.

TABLE II
DESIGN SPACE FOR OPTIMAL THERMOELECTRIC PERFORMANCE OF N-TYPE GAAS NWS.

OR	PF		ZT	
	STR	CS	STR	CS
Dev.I	Weak improvement ∼	Small size better	Weak improvement ∼	Small size better
Dev.II	Strong improvement ↑	Small size better	Strong improvement ↑	Small size better
Dev.III	Strong improvement ↑	Small size better	Weak improvement ∼	Small size better
Dev.IV	Weak improvement ∼	Small size better	Weak improvement ∼	Small size better
Dev.V	Weak improvement ∼	Small size better	Weak improvement ∼	Small size better
Dev.VI	Strong improvement ↑	Small size better	Strong improvement ↑	Small size better

with [110] transport orientation provide a improvement in the ZT and PF compared to the other wafer and wire orientations. Wire cross-section sizes below 6nm are more conducive to ZT and PF enhancement under strain due to suppressed electron scattering resulting from the interplay of the geometrical confinement and the uniaxial strain.

ACKNOWLEDGEMENT

Financial supports from MSD under SRC, NRI under MIND and NSF are gratefully acknowledged. Computational support from nanoHUB.org, supported by NSF and managed by NCN is also acknowledged.

REFERENCES

[1] P. N. Martin, Z. Aksamija, E. Pop, and U. Ravaioli, "Reduced thermal conductivity in nanoengineered rough ge and gaas nanowires," *Nano Letters*, vol. 10, no. 4, pp. 1120–1124, 2010, pMID: 20222669. [Online]. Available: http://pubs.acs.org/doi/abs/10.1021/nl902720v

[2] S. Barman and G. P. Srivastava, "Thermal conductivity of suspended *GaAs* nanostructures: Theoretical study," *Phys. Rev. B*, vol. 73, no. 20, p. 205308, May 2006.

[3] P. Solomon and S. Laux, "The ballistic fet: design, capacitance and speed limit," in *Electron Devices Meeting, 2001. IEDM Technical Digest. International*, Dec. 2001, pp. 5.1.1 –5.1.4.

[4] A. I. Hochbaum, R. Chen, R. D. Delgado, W. Liang, E. C. Garnett, M. Najarian, A. Majumdar, and P. Yang, "Enhanced thermoelectric performance of rough silicon nanowires," *Nature*, vol. 451, pp. 163–167, 2008.

[5] M. Soini, I. Zardo, E. Uccelli, S. Funk, G. Koblmüller, A. F. i Morral, and G. Abstreiter, "Thermal conductivity of gaas nanowires studied by micro-raman spectroscopy combined with laser heating," *Applied Physics Letters*, vol. 97, no. 26, p. 263107, 2010. [Online]. Available: http://link.aip.org/link/?APL/97/263107/1

[6] C. Jeong, R. Kim, M. Luisier, S. Datta, and M. Lundstrom, "On Landauer versus Boltzmann and full band versus effective mass evaluation of thermoelectric transport coefficients," *Journal of Applied Physics*, vol. 107, no. 2, p. 023707, 2010.

[7] P. Grivickas, M. D. McCluskey, and Y. M. Gupta, "Transformation of gaas into an indirect l -band-gap semiconductor under uniaxial strain," *Phys. Rev. B*, vol. 80, no. 7, p. 073201, Aug 2009.

[8] M. Rodwell, W. Frensley, S. Steiger, E. Chagarov, S. Lee, H. Ryu, Y. Tan, G. Hegde, L. Wang, J. Law, T. Boykin, G. Klimek, P. Asbeck, A. Kummel, and J. Schulman, "Iii-v fet channel designs for high current densities and thin inversion layers," in *Device Research Conference (DRC), 2010*, june 2010, pp. 149 –152.

[9] C. Gutsche, A. Lysov, I. Regolin, K. Blekker, W. Prost, and F.-J. Tegude, "Controllable p-type doping of GaAs nanowires during vapor-liquid-solid growth," *Journal of Applied Physics*, vol. 105, no. 024305, 2009.

[10] ——, "n-Type Doping of VaporLiquidSolid Grown GaAs Nanowires," *Nanoscale Res. Letter*, vol. 6, 2011.

[11] D. Nakata, H. Shibata, Y. Shiratori, and S. Kasai, "Voltage Transfer Characteristics in GaAs-Based Three-Branch Nanowire Junctions Controlled by Schottky Wrap Gates," *Jap. Jour. of App. Phys.*, vol. 49, no. 06GG03, 2010.

[12] D. Spirkoska, C. Colombo, M. Heiss, G. Abstreiter, and A. F. i Morral, "The use of molecular beam epitaxy for the synthesis of high purity iiiv nanowires," *Journal of Physics: Condensed Matter*, vol. 20, no. 45, p. 454225, 2008. [Online]. Available: http://stacks.iop.org/0953-8984/20/i=45/a=454225

[13] A. I. Persson, M. W. Larsson, S. Stenstrom, B. J. Ohlsson, L. Samuelson, and L. R. Wallenberg, "Solid-phase diffusion mechanism for GaAs nanowire growth," *Nature Materials*, vol. 3, pp. 677– 681, 2004.

[14] R. Landauer, "Spatial Variation of Currents and Fields Due to Localized Scatterers in Metallic Conduction," *IBM Journal of Research and Development*, vol. 1, no. 3, pp. 223 –231, july 1957.

[15] S. Datta, "Electronic Transport in Mesoscopic Systems," *Cambridge University Press, New York*, p. 393, 1997.

[16] N. Mingo, "Thermoelectric figure of merit and maximum power factor in iii–v semiconductor nanowires," *Applied Physics Letters*, vol. 84, no. 14, pp. 2652–2654, 2004.

[17] T. T. Vo, A. J. Williamson, V. Lordi, and G. Galli, "Atomistic design of thermoelectric properties of silicon nanowires," *Nano Letters*, vol. 8, no. 4, pp. 1111–1114, 2008.

[18] G. Klimeck, F. Oyafuso, T. B. Boykin, R. C. Bowen, and P. v. Allmen, "Development of a Nanoelectronic 3-D (NEMO 3-D) Simulator for Multimillion Atom Simulations and Its Application to Alloyed Quantum Dots," *Computer Modeling in Engineering and Science (CMES)*, vol. 3, no. 5, pp. 601–642, 2002.

[19] T. B. Boykin, M. Luisier, M. Salmani-Jelodar, and G. Klimeck, "Strain-induced, off-diagonal, same-atom parameters in empirical tight-binding theory suitable for [110] uniaxial strain applied to a silicon parametrization," *Phys. Rev. B*, vol. 81, no. 12, p. 125202, 2010.